

Unexpected Behavior of Heavy-Ion Fusion Cross Sections at Extreme Sub-Barrier Energies

C. L. Jiang, H. Esbensen, K. E. Rehm, B. B. Back, R. V. F. Janssens, J. A. Caggiano, P. Collon, J. Greene, A. M. Heinz, D. J. Henderson, I. Nishinaka, T. O. Pennington, and D. Seweryniak

Physics Division, Argonne National Laboratory, Argonne, Illinois 60439

(Received 9 January 2002; published 11 July 2002)

The excitation function for fusion evaporation in the $^{60}\text{Ni} + ^{89}\text{Y}$ system was measured over a range in cross section covering 6 orders of magnitude. The cross section exhibits an abrupt decrease at extreme sub-barrier energies. This behavior, which is also present in a few other systems found in the literature, cannot be reproduced with present models, including those based on a coupled-channels approach. Possible causes are discussed, including a dependence on the intrinsic structure of the participants.

DOI: 10.1103/PhysRevLett.89.052701

PACS numbers: 25.70.Jj, 24.10.Eq, 25.60.-t, 25.70.Gh

Fusion cross sections between heavy ions at sub-barrier energies have been studied extensively since it was realized that, near and below the Coulomb barrier, the measured yields are strongly enhanced compared to one-dimensional tunneling calculations [1,2]. This enhancement has been explained in terms of channel-coupling effects which create a multidimensional potential barrier and result in increased fusion probabilities. In most experiments carried out thus far, fusion cross sections have been measured down to the 0.1–1 mb level, and coupled-channels calculations have proven quite successful in reproducing the general trends of the measured yields [3]. At these energies, measurements of fusion cross sections are sometimes interpreted in terms of a barrier distribution $B(E)$, which is extracted from the second derivative, $d^2(\sigma E)/dE^2$, of the product of the fusion cross section σ and the center-of-mass energy E [2,4].

The present work deals with fusion cross sections well below 0.1 mb. Naively, one would expect coupled-channels effects to saturate at low bombarding energies and the product σE to exhibit a simple exponential falloff with decreasing energy [1,5]. Here, we show that the low-energy data, near the low-energy-edge of the barrier distribution, often exhibit a decrease much steeper than anticipated, and much steeper than predicted by a simple exponential falloff. It is worth pointing out that this phenomenon is of particular interest for fusion reactions of astrophysical interest, as these usually take place at extreme sub-barrier energies.

Two examples of fusion evaporation excitation functions which have been measured to very small cross sections are shown in Fig. 1(a), where they are plotted as σE versus E/V_b with the Coulomb barrier V_b calculated from the systematics of Ref. [6]. The solid line is the result of coupled-channels calculations in the case of $^{58}\text{Ni} + ^{58}\text{Ni}$ (similar to those of Ref. [7]). Such calculations are, however, not yet available for reactions between heavier nuclei such as the $^{90}\text{Zr} + ^{92}\text{Zr}$ system shown in Fig. 1(a). In these instances the Wong formula [8] is used here as a representation of the data. The latter formula has been introduced successfully in many analyses of heavy-ion induced fusion

data [1,4,9]. In the case of $^{58}\text{Ni} + ^{58}\text{Ni}$, it can be seen that this description compares well with the results of the coupled-channels calculations. It is clear from Fig. 1(a) that the exponential slope of the data at the low energies exhibits a continuous change with decreasing energy rather than a constant slope. Most importantly, at the lowest energies, the falloff is steeper than predicted by the theoretical models. It should be noted that for the two systems contributions from fusion-fission reactions can be neglected at these low energies [10,11].

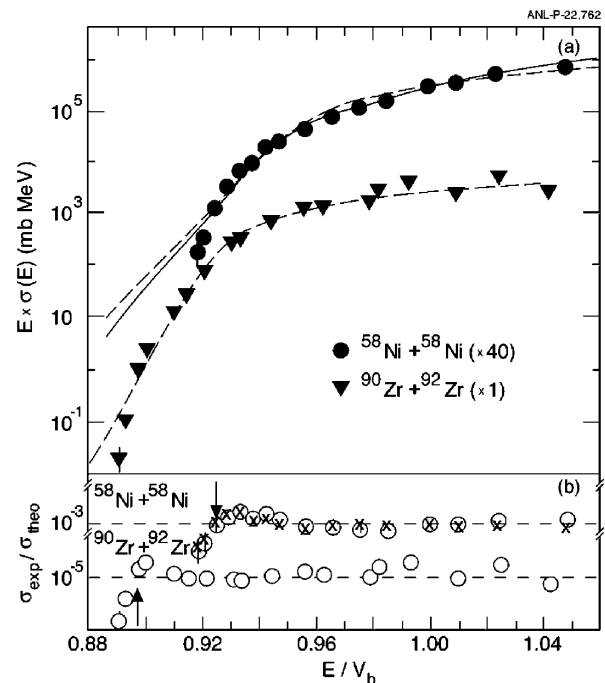


FIG. 1. (a) Plots of σE versus E/V_b for the systems $^{58}\text{Ni} + ^{58}\text{Ni}$ and $^{90}\text{Zr} + ^{92}\text{Zr}$. The lines are the results of either coupled-channels calculations (solid) or a phenomenological description with the Wong formula (dashed). See text for details. (b) $\sigma_{\text{exp}}/\sigma_{\text{theo}}$ vs E/V_b ; circles: σ_{theo} calculated using the Wong formula; crosses: σ_{theo} calculated within the coupled-channels formalism.

To amplify the low-energy behavior of the cross sections, we present in Fig. 1(b) the ratio of the experimental cross sections and either the results of coupled-channels calculations, where available, or, again, of the parametrization based on the Wong formula. The parameters used in the Wong formula for $^{90}\text{Zr} + ^{92}\text{Zr}$ are $\hbar\omega_0 = 5.43$ MeV and $V_w = 175.6$ MeV for the fusion barrier. The corresponding values for $^{58}\text{Ni} + ^{58}\text{Ni}$ are $\hbar\omega_0 = 4.22$ MeV and $V_w = 96.2$ MeV. The coupled-channels calculations include one- and two-phonon couplings to the low-lying 2^+ and 3^- states in ^{58}Ni just as in Ref. [7], but the nuclear quadrupole coupling is 12% larger, and the radius of the nuclear potential has been adjusted to minimize the χ^2 , which is 3.0. This minimum χ^2 is reduced to a value of 1.3 if the two lowest energy points are excluded from the fit. While these descriptions give good agreement with the data at higher energies, they are unable to reproduce the yields at the lowest energies, where one observes a dropoff in the cross-section ratio starting at an energy E_0 indicated by the arrows. In the case of $^{90}\text{Zr} + ^{92}\text{Zr}$, this can again be illustrated by the measured χ^2 value which improves from 14 to 5 when the lowest energy data point is not included in the fit. Four systems exhibiting this unexpected behavior have been found in the literature. They are $^{58}\text{Ni} + ^{58}\text{Ni}$ [12], $^{90}\text{Zr} + ^{90}\text{Zr}$, ^{92}Zr , and ^{89}Y [13].

It should be noted that precise measurements of very small fusion cross sections are experimentally challenging. Reactions on small amounts of heavier isotopic target contaminants can dominate the low-energy yields due to their higher center-of-mass energies. In addition, even rare isobaric contaminants in the beam (e.g., a ^{58}Fe contamination in a ^{58}Ni beam) can sharply affect the fusion cross sections at the lowest energies because of the strong dependence of these cross sections on the respective Coulomb barriers. For these reasons some systems have not been included in the compilation mentioned above.

The energy E_0 at which the dropoff occurs can be extracted from the data with a relative error of about 2%. Because of the limited amount of data, especially between $V_b = 100$ –178 MeV, we have chosen the system $^{60}\text{Ni} + ^{89}\text{Y}$ for a new measurement of fusion cross sections at very low energies. An additional reason for choosing this system is that neither the beam nor the target has isobaric or isotopic contaminants.

The experiment was performed at the Argonne superconducting linear accelerator ATLAS with a $100 \mu\text{g}/\text{cm}^2$ yttrium target evaporated on a thin carbon foil ($100 \mu\text{g}/\text{cm}^2$). The evaporation residues escaping from the target were detected at $\theta_{\text{lab}} = 0 \pm 2.3^\circ$ with the fragment mass analyzer (FMA) [14]. At the focal plane of this instrument the residues, dispersed according to their mass-to-charge ratio M/Q , were detected by an x - y , position-sensitive, parallel grid avalanche counter (PGAC) followed by a large volume ionization chamber (IC) and a silicon detector. The position signal was used for the M/Q determination. Five energy signals (one from the PGAC, three from the IC, and one from the silicon detec-

tor), and two time-of-flight signals (from the target to the PGAC, and from the PGAC to the silicon detector) were used to discriminate residues from the background originating mostly from scattered beam particles. Two surface barrier silicon detectors, positioned at 45° and 60° with respect to the beam, served to monitor the beam and the target condition. Only residues with two charge states were detected simultaneously at the focal plane. This was taken into account in the analysis by measuring the full charge state distribution at several energies. In combination with theoretical parametrizations, this procedure was sufficient to determine at each beam energy the charge state fraction of the detected evaporation residues. The transport efficiency of the FMA was calculated with Monte Carlo simulations using a modified version of the GIOS code [15]. The recoil energy and the angular distribution of the residues were calculated with the statistical model code PACE [16]. The large momentum acceptance, $\pm 10\%$, and the large angular acceptance, $\theta_{\text{lab}} < 2.3^\circ$, of the FMA result in a high detection efficiency for the residues (~ 50 – 70% for each charge state detected). Representative M/Q spectra for $Q = 23$ obtained at three center-of-mass energies ($E = 123.5, 122.1, 121.4$ MeV), are presented in the inset of Fig. 2. At $E = 123.5$ MeV, a strong peak for mass 147 and smaller

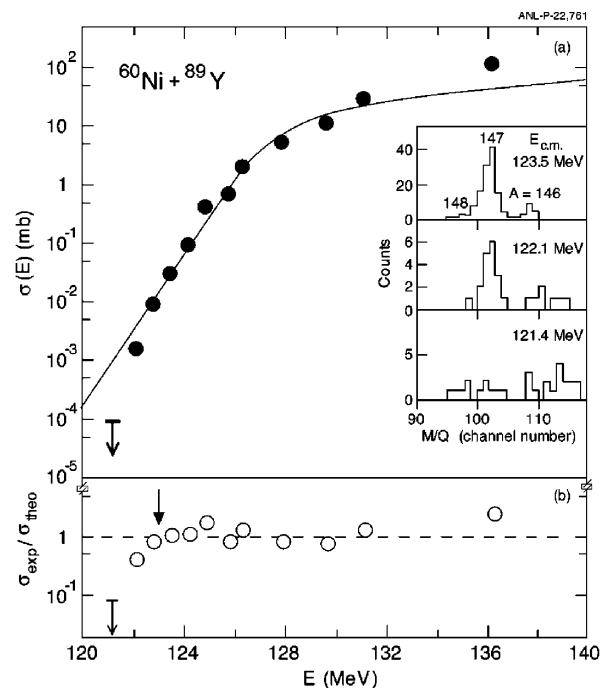


FIG. 2. Experimental evaporation residue cross sections $\sigma(E)$, (a) and $\sigma_{\text{exp}}/\sigma_{\text{theo}}$, (b) (σ_{theo} calculated from the Wong formula), plotted as a function of the center-of-mass energy for the system $^{60}\text{Ni} + ^{89}\text{Y}$. The incident energies have been corrected for the finite target thickness (including the influence of sharp changes in the excitation function with energy). The uncertainties in the cross sections are smaller than the points. Only an upper limit to the cross section was obtained at the lowest energy. The inset presents M/Q spectra obtained at three center-of-mass energies.

contributions for $A = 148$ and 146 are observed free of background. At 122.1 MeV, the second lowest energy measured here, a small background shows up, which can be readily separated. At the lowest beam energy, even in a 16 h run no clear signal for evaporation residues could be identified above the background, and only an upper limit of 95 nb was derived for the cross section. The uncertainties in the absolute cross sections include a systematic error of $\sim 10\%$ associated with the possible production of residues with longer-lived isomers which may be lost if the decay occurs in flight inside the FMA. However, this effect should not influence the relative values of the excitation function since no apparent change in the shape of the charge state distributions was observed in the range of incident energies under consideration.

The excitation function for evaporation residue production in the system $^{60}\text{Ni} + ^{89}\text{Y}$, covering cross sections from about 100 mb to less than 100 nb, is presented in Fig. 2(a). Also indicated in the figure are the results of a calculation using the Wong parametrization (with $\hbar\omega_0 = 4.16$ MeV and $V_w = 126.6$ MeV). Excluding the lowest two energy points, a satisfactory χ^2 value of 4 is obtained just as in the cases discussed above ($\chi^2 = 9$ with the lower points included). At the lowest energies the experimental cross sections again fall below the calculated values, as is best seen from the ratio $\sigma_{\text{exp}}/\sigma_{\text{theo}}$ given in Fig. 2(b), and an energy E_0 [see arrow in Fig. 2(b)] can be derived. Remarkably, the data for the five available systems indicate that the onset of the steeper than expected decrease in the fusion cross section can be parametrized by the relation $E_0 \sim 0.91V_b$. This observation may well suggest that this reduction in cross section is an entrance channel effect.

Another way to illustrate the steep falloff in the σE product is to examine the exponential slopes defined as $L(E) = d(\ln(\sigma E))/dE$. These are plotted as a function of E/E_0 for three systems in Fig. 3. In addition to straightforward determinations from consecutive data points, slopes were also derived from least-squares fits to three data points in an attempt to avoid fluctuations which may arise as a result of large errors on small cross sections or of uncertainties in the determination of the beam energy. In Fig. 3, the slopes determined from two or three consecutive points are given as solid circles and stars, respectively, at the corresponding average energies. The dashed and solid lines in the figure represent the results of coupled-channels calculations and of the Wong formula, respectively. While the calculated slopes approach a constant value of ~ 1.5 MeV $^{-1}$, the experimental data exhibit a continuous increase with decreasing energies. Thus, at least two representations of the experimental effect are possible. It would clearly be of great interest to investigate whether the behavior observed here persists at even lower energies.

The values of E_0 , the compound nucleus excitation energy E_{ex} , the ratio $E_0/0.91V_b$, and the cross sections at the energy E_0 are summarized in Table I for the five systems. There are also two systems, $^{50}\text{Ti} + ^{208}\text{Pb}$ [17] and $^{64}\text{Ni} + ^{64}\text{Ni}$ [18], for which a steep falloff in σE is

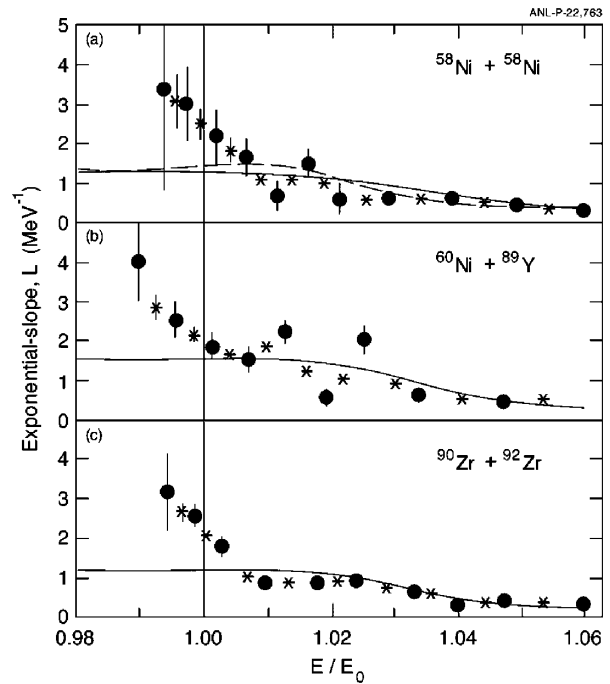


FIG. 3. Exponential slopes $L(E)$, $d[\ln(\sigma E)]/dE$, plotted as a function of E/E_0 for the systems $^{58}\text{Ni} + ^{58}\text{Ni}$, $^{60}\text{Ni} + ^{89}\text{Y}$, and $^{90}\text{Zr} + ^{92}\text{Zr}$. Solid circles and stars correspond to slope determinations from consecutive data points and from least-squares fits to three data points, respectively. Solid and dashed lines are the results of theoretical calculations with the Wong formula and the coupled-channel formalism, respectively.

observed, although it is apparent only at the lowest data point. These systems are included in the second part of Table I. It should also be noted that many systems can be found in the literature which show an increase in the exponential slope with decreasing energy, although in these instances the measurements do not extend to sufficiently low energies to exhibit the falloff in σE explicitly. Some of these systems are included in Table I as well, especially those for which the cross sections have been measured to rather low values. In these cases, the quoted values of E_0 and $\sigma(E_0)$ correspond to the lowest energies measured in the respective experiments.

As can be seen from the third column in Table I, those systems involving closed-shell (“stiff”) nuclei in the entrance channel are usually well described by the systematics $E_0 \sim 0.91V_b$. For reactions involving open-shell (“soft”) nuclei in the entrance channel, firm E_0 values are not yet available, and the upper limits given in Table I suggest that there is a nuclear structure dependence to this phenomenon. It is likely that the larger channel-coupling effects for these softer participants are pushing the appearance of the phenomenon towards lower E_0/V_b values.

It should be noted that the energy E_0 and the associated onset of an increase in the exponential slope $L(E)$ are located in the low-energy tail of the barrier distribution $B(E)$. However, there does not appear to be a precise relationship between E_0 [or $L(E_0)$] and this low-energy

TABLE I. Dropoff energy E_0 and other relevant information for various systems. In each case V_b is the barrier height calculated from the formula given by Vaz *et al.* [6]. The symbols $E_{\text{ex}}(E_0)$ and $\sigma(E_0)$ refer to the excitation energy of the compound system and the fusion evaporation cross section at the energy E_0 . The values of E_0 , $E_{\text{ex}}(E_0)$, and $\sigma(E_0)$ for the last 12 rows correspond to the lowest energy measured in the respective experiments. In these cases E_0 should be regarded as an upper limit only.

System	E_0		$E_{\text{ex}}(E_0)$ MeV	$\sigma(E_0)$ mb	Ref.
	MeV	$E_0/0.91V_b$			
$^{58}\text{Ni} + ^{58}\text{Ni}$	93.9	1.02 ± 0.02	27.8	0.40	[12]
$^{60}\text{Ni} + ^{89}\text{Y}$	123.0	1.02 ± 0.02	32.5	0.009	Present
$^{90}\text{Zr} + ^{89}\text{Y}$	170.8	1.00 ± 0.02	19.3	0.20	[13]
$^{90}\text{Zr} + ^{92}\text{Zr}$	170.8	0.99 ± 0.02	17.1	0.006	[13]
$^{90}\text{Zr} + ^{90}\text{Zr}$	175.2	1.00 ± 0.02	17.9	0.020	[13]
$^{50}\text{Ti} + ^{208}\text{Pb}$	181.6	0.98	12.0	0.003	[17]
$^{64}\text{Ni} + ^{64}\text{Ni}$	89.2	1.00	40.4	0.02	[18]
$^{16}\text{O} + ^{208}\text{Pb}$	70.1	1.01	23.6	0.39	[19]
$^{40}\text{Ca} + ^{90}\text{Zr}$	94.3	1.01	36.1	0.84	[20]
$^{16}\text{O} + ^{144}\text{Sm}$	56.6	1.01	28.1	0.15	[21]
$^{19}\text{F} + ^{208}\text{Pb}$	75.1	0.96	24.9	0.023	[22]
$^{16}\text{O} + ^{154}\text{Sm}$	52.4	0.95	36.0	0.18	[21]
$^{40}\text{Ar} + ^{144}\text{Sm}$	116.6	0.96	25.8	0.0016	[23]
$^{40}\text{Ar} + ^{154}\text{Sm}$	108.8	0.91	33.5	0.0016	[23]
$^{40}\text{Ar} + ^{112}\text{Sn}$	96.6	0.96	33.5	0.0084	[23]
$^{40}\text{Ar} + ^{122}\text{Sn}$	94.0	0.95	35.4	0.0018	[23]
$^{86}\text{Kr} + ^{92}\text{Mo}$	160.4	0.98	22.3	0.007	[24]
$^{86}\text{Kr} + ^{104}\text{Ru}$	162.4	0.96	23.9	0.0049	[24]
$^{36}\text{S} + ^{110}\text{Pd}$	79.7	0.97	41.7	0.0021	[25]

tail. While the exponential slopes emphasize the behavior of σE at very low energies (even lower than E_0), this behavior is hard to infer from the barrier distributions. This can be seen from the relation

$$B(E) = \sigma E \left[\frac{dL(E)}{dE} + (L(E))^2 \right],$$

which follows from the definitions of $L(E)$ and $B(E)$. Indeed, an anomalous behavior in $dL(E)/dE$ at very low energies will be suppressed in the barrier distribution by the second term $[L(E)]^2$ and the overall factor σE .

Some aspects of the behavior of the cross sections at low energies can be understood on the basis of the underlying Q values, while others remain unexplained. In fusion reactions between two heavy ions, the reaction Q values are always negative. As a result, once the excitation energy in the compound system E_{ex} reaches zero, which occurs at a finite bombarding energy, the cross section must be zero, and thus the exponential slope of σE should approach infinity. Hence, for a heavy-ion system, the slope $L(E)$ should increase towards infinity with decreasing energy. Any theoretical model attempting to describe the fusion behavior at extreme sub-barrier energies should include the properties of the fused system as expressed through the Q

value. The Q value alone is, however, not sufficient to explain the phenomenon explored in this study. Present fusion models assume that the fused system can be populated at the excitation energy and spin corresponding to the entrance channel kinetic energy and angular momentum. This assumption is valid only as long as the total width of the compound state remains larger than the level spacing. When this condition is not satisfied a reduction of the fusion probability ensues, as is well known from capture reactions with thermal neutrons. For most of the systems under study here, however, the falloff of the cross sections occurs at excitation energies $E_{\text{ex}} \sim 20\text{--}30$ MeV where the level densities are still very high. These observations argue for another physical reason for reduced penetration or another hindrance implied by the negative Q value; the most likely being an entrance channel phenomenon. More low-energy cross-section measurements for both fusion evaporation and fusion-fission are needed to fully understand this interesting behavior, in particular, for soft systems.

The authors thank J. P. Schiffer and A. H. Wuosmaa for valuable discussions. This work was supported by the U.S. Department of Energy, Nuclear Physics Division, under Contract No. W-31-109-ENG-38.

- [1] R. Vandenbosch, *Annu. Rev. Nucl. Part. Sci.* **42**, 447 (1992).
- [2] M. Dasgupta *et al.*, *Annu. Rev. Nucl. Part. Sci.* **48**, 401 (1998).
- [3] K. Hagino and N. Takigawa, *Phys. Rev. C* **55**, 276 (1997).
- [4] N. Rowley, G. R. Satchler, and P. H. Stelson, *Phys. Lett. B* **254**, 25 (1991).
- [5] J. Fernández-Niello, C. H. Dasso, and S. Landowne, *Comput. Phys. Commun.* **54**, 409 (1989).
- [6] L. C. Vaz and J. M. Alexander, *Phys. Rep.* **69**, 373 (1981).
- [7] H. Esbensen and S. Landowne, *Phys. Rev. C* **35**, 2090 (1987).
- [8] C. Y. Wong, *Phys. Rev. Lett.* **31**, 766 (1973).
- [9] U. Jahnke *et al.*, *Phys. Rev. Lett.* **48**, 17 (1982).
- [10] K. T. Lesko *et al.*, *Phys. Rev. C* **34**, 2155 (1986).
- [11] C. R. Morton *et al.*, *Phys. Rev. C* **62**, 024607 (2000).
- [12] M. Beckerman *et al.*, *Phys. Rev. C* **25**, 837 (1982).
- [13] J. G. Keller *et al.*, *Nucl. Phys.* **A452**, 173 (1986).
- [14] C. N. Davids and J. Larson, *Nucl. Instrum. Methods Phys. Res., Sect. B* **40/41**, 1224 (1989); *Nucl. Instrum. Methods Phys. Res., Sect. A* **345**, 528 (1994).
- [15] C. L. Jiang and C. N. Davids, *ANL Physics Division Annual Report No. ANL-95/14*, p. 74.
- [16] A. Gavron, *Phys. Rev. C* **21**, 230 (1980).
- [17] S. Hofmann *et al.*, *Z. Phys. A* **358**, 377 (1997).
- [18] D. Ackermann *et al.*, *Nucl. Phys.* **A609**, 91 (1996).
- [19] C. R. Morton *et al.*, *Phys. Rev. C* **60**, 044608 (1999).
- [20] H. Timmers *et al.*, *Nucl. Phys.* **A633**, 421 (1998).
- [21] J. R. Leigh *et al.*, *Phys. Rev. C* **52**, 3151 (1995).
- [22] D. J. Hinde *et al.*, *Phys. Rev. C* **60**, 054602 (1999).
- [23] W. Reisdorf *et al.*, *Nucl. Phys.* **A438**, 212 (1985).
- [24] W. Reisdorf *et al.*, *Nucl. Phys.* **A444**, 154 (1985).
- [25] A. M. Stefanini *et al.*, *Phys. Rev. C* **52**, R1727 (1995).